

Super-Eddington Magnetized Neutron Star Accretion Flows: a Self-similar Analysis

KEN CHEN¹ AND ZI-GAO DAI²

¹*School of Astronomy and Space Science, Nanjing University, Nanjing 210023, China*

²*Department of Astronomy, University of Science and Technology of China, Hefei 230026, China; daizg@ustc.edu.cn*

ABSTRACT

The properties of super-Eddington accretion disks exhibit substantial distinctions from the sub-Eddington ones. In this paper, we investigate the accretion process of a magnetized neutron star (NS) surrounded by a super-Eddington disk. By constructing self-similar solutions for the disk structure, we study in detail an interaction between the NS magnetosphere and the inner region of the disk, revealing that this interaction takes place within a thin boundary layer. The magnetosphere truncation radius is found to be approximately proportional to the Alfvén radius, with a coefficient ranging between 0.34 – 0.71, influenced by the advection and twisting of a magnetic field, NS rotation, and radiation emitted from an NS accretion column. Under super-Eddington accretion, the NS can readily spin up to become a rapid rotator. The proposed model can be employed to explore the accretion and evolution of NSs in diverse astrophysical contexts, such as ultraluminous X-ray binaries or active galactic nucleus disks.

Keywords: Compact object (288); Neutron stars (1108); Accretion (14)

1. INTRODUCTION

Accretion is a widespread process occurring in various neutron star (NS) systems, such as newborn NSs within supernova envelopes (e.g. [Chevalier 1989](#)), NSs in high-mass X-ray binaries (e.g. [Reig 2011](#)), and NSs in low-mass X-ray binaries (e.g. [Bhattacharya & van den Heuvel 1991](#)), among others, contributing significantly to the evolution of the mass, spin, and magnetic field properties of the NSs (e.g. [Konar 2017](#); [Igoshev et al. 2021](#); [Abolmasov et al. 2024](#)), while concurrently producing observable radiation (e.g. [Mushtukov & Tsygankov 2022](#); [Ascenzi et al. 2024](#)). Therefore, accretion plays a crucial role in the NS populations ([Harding 2013](#)). The accretion of the NS is distinctive. Due to the inherent magnetization of the NS, accreting matter is blocked by the NS magnetosphere from falling freely onto its solid surface, but can penetrate into the magnetosphere via instability and subsequently flows along the field lines toward the NS magnetic poles (e.g. [Bozzo et al. 2008](#); [Shakura & Postnov 2017](#); [Fornasini et al. 2023](#)). Additionally, a circum-NS disk can form when the accretion material possesses angular momentum, leading to a slightly more complicated accretion process (e.g. [Romanova & Owocki 2015](#)).

So far, the majority of studies have primarily focused on sub-Eddington magnetized NS accretion systems, characterized by a thin and approximately Keplerian rotating circum-NS disk. However, there exist astrophysical scenarios that involve super-Eddington disk-accreting NSs. Recently, the discovery of ultraluminous X-ray pulsars (ULXPs) with apparent luminosities ranging between $10^{39} - 10^{41}$ erg s⁻¹, although with uncertain geometrical beaming ([Lasota & King 2023](#)), implies the existence of super-Eddington NS accretion systems ([Fabrika et al. 2021](#); [King et al. 2023](#)). Besides, NSs are predicted to widely reside in active galactic nucleus (AGN) disks (e.g. [McKernan et al. 2020](#); [Tagawa et al. 2021](#); [Perna et al. 2021](#)), where the environment is extremely dense and differentially rotating (e.g. [Sirko & Goodman 2003](#)), thereby leading to a super-Eddington disk accretion of the NS (e.g. [Pan & Yang 2021](#); [Chen et al. 2023](#)). In contrast to the standard thin accretion disk, the super-Eddington disk exhibits distinctive properties, in that it is geometrically thick, sub-Keplerian in rotation, and advection-dominated in cooling (e.g. [Abramowicz et al. 1988](#)); additionally, the accretion process is always accompanied by a powerful outflow to reduce the inward inflow mass rate ([Blandford & Begelman 1999](#); [Gu 2015](#)). Therefore, it is imperative to conduct a comprehensive study of the super-Eddington magnetized NS accretion system, enabling us to explore specific properties of NS accretion and the evolution of the NS driven by a super-Eddington flow. Several works have both analytically and numerically

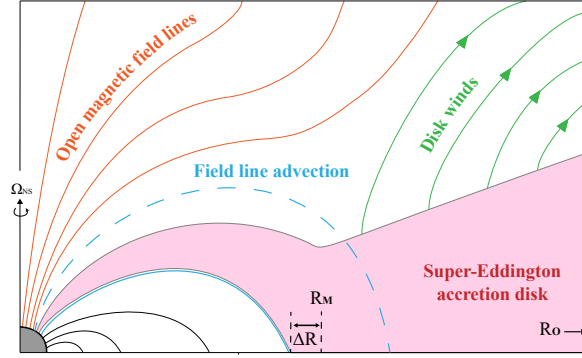


Figure 1. Schematic diagram illustrating the super-Eddington disk accretion process of a magnetized rotating NS, where the certain object is an NS, Ω_{NS} is the NS spin rate, R_{M} denotes the magnetosphere truncation radius, ΔR represents the thickness of the interaction boundary layer, and R_{o} is the disk outer boundary, which is simplified set to be smaller than R_{tr} , indicating that the launching of disk winds occurs throughout the entire disk region. Some NS closed magnetic field lines, depicted by the blue dashed line, would undergo inward advection within the super-Eddington disk. Consequently, these field lines become concentrated at the magnetosphere-disk interaction layer, as indicated by the blue line, leading to an increase in magnetic pressure. It should be noted that the schematic serves solely for illustrative purposes and does not accurately depict the relative scale of the system components, while also the interaction between the NS open field lines and the disk winds is disregarded.

investigated the accretion structure of this system (e.g. Ohsuga 2007; Takahashi & Ohsuga 2017; Chashkina et al. 2017, 2019; Abarca et al. 2021; Inoue et al. 2023).

In this paper, we investigate the super-Eddington accretion process of a magnetized NS by constructing a generalized super-Eddington circum-NS disk with varying strengths of the disk wind, particularly focusing on an interaction between the NS magnetosphere and the inner disk. A schematic diagram of the accretion system is shown in Figure 1. This paper is organized as follows. In Section 2, we present a self-similar solution to describe the structure of a super-Eddington disk. The specific magnetosphere-disk interaction process, as well as the resulting NS accretion properties, are shown in Section 3. Several discussions are provided in Section 4. Our conclusions are summarized in Section 5. The terms c and G in this paper denote the speed of light and the gravitational constant, respectively. The mass of an NS is taken to be $1.4M_{\odot}$ in the paper.

2. SUPER-EDDINGTON ACCRETION DISK

2.1. Disk Equations

In a super-Eddington accretion disk, internal photons are trapped because of a dense gas obstructing their vertical diffusion. A large amount of photons and energy can be advected inward with the gas inflow, rather than escape as radiation. When the timescale of photon vertical diffusion exceeds that of disk accretion, the radiation-effective flow converts to be radiation-ineffective roughly at the trapping radius (e.g. Kato et al. 2008; Kitaki et al. 2021):

$$R_{\text{tr}} = 3\dot{m}hR_{\text{g}}, \quad (1)$$

where $\dot{m} = \dot{M}/\dot{M}_{\text{Edd}}$ is the dimensionless mass inflow rate of the disk, $\dot{M}_{\text{Edd}} = L_{\text{Edd}}/c^2$ is the Eddington limit accretion rate, $L_{\text{Edd}} = 4\pi GMm_{\text{p}}c/\sigma_{\text{T}} = 1.26 \times 10^{38} m \text{ erg s}^{-1}$, $m = M/M_{\odot}$ is the dimensionless mass of the NS, m_{p} is the proton mass, σ_{T} is the Thompson cross section, $h = H/R$ is the height ratio of the disk, and $R_{\text{g}} = GM/c^2$ is the gravitational radius. Inside R_{tr} , the trapped photons exert strong radiation pressure, which can induce disk winds to remove mass, angular momentum, and energy from the accretion disk (Ohsuga & Mineshige 2007).

Containing the contribution of an outflow, the equation of continuity is written as

$$\frac{1}{R} \frac{d}{dR} (R\Sigma V_{\text{R}}) + \frac{1}{2\pi R} \frac{d\dot{M}_{\text{w}}}{dR} = 0, \quad (2)$$

where $\Sigma = 2\rho H$, ρ , and V_{R} are the surface density, density, and radial inflow velocity of the disk, respectively, and the outflow mass-loss rate \dot{M}_{w} is

$$\dot{M}_{\text{w}}(R) = \int_{R_{\text{in}}}^R 4\pi R' \dot{m}_{\text{w}}(R') dR', \quad (3)$$

where R_{in} denotes the radius of the disk inner edge and \dot{m}_{w} is the mass-loss rate per unit area from each disk face.

The integrated radial momentum equation and the azimuthal equation of motions, respectively, can be written by

$$V_{\text{R}} \frac{dV_{\text{R}}}{dR} + (\Omega_{\text{K}}^2 - \Omega^2) R + \frac{1}{\rho} \frac{dP}{dR} = 0, \quad (4)$$

$$-\frac{1}{R} \frac{d}{dR} (R^3 \Sigma V_{\text{R}} \Omega) + \frac{1}{R} \frac{d}{dR} \left(R^3 \nu \Sigma \frac{d\Omega}{dR} \right) - \frac{(lR)^2 \Omega}{2\pi R} \frac{d\dot{M}_{\text{w}}}{dR} = 0, \quad (5)$$

where P and $\nu = -\alpha P / (\rho R d\Omega/dR)$ are the pressure and viscosity of the disk, α is the viscosity parameter (Shakura & Sunyaev 1973), and Ω_{K} is the Keplerian angular velocity. In the last term of Equation (5), $l \geq 1$ quantifies the specific angular momentum carried away by the disk wind, where $l = 1$ represents the outflow removing the local disk angular momentum at its originating radius (e.g. Knigge 1999; Proga 2000).

The energy equation is

$$Q_{\text{vis}} = Q_{\text{adv}} + Q_{\text{rad}} + Q_{\text{w}}, \quad (6)$$

where Q_{vis} , Q_{adv} , and Q_{rad} are the viscous heating rate, the advection cooling rate, and the radiation cooling rate per unit area, respectively, for which the expressions are as follows (e.g. Abramowicz et al. 1995; Sirko & Goodman 2003):

$$Q_{\text{vis}} = \nu \Sigma \left(R \frac{d\Omega}{dR} \right)^2, \quad (7)$$

$$Q_{\text{adv}} = \Sigma V_{\text{R}} T \frac{dS}{dR} = \Sigma V_{\text{R}} \left(\frac{1}{\gamma - 1} \frac{dc_{\text{s}}^2}{dR} - \frac{c_{\text{s}}^2}{\rho} \frac{d\rho}{dR} \right), \quad (8)$$

$$Q_{\text{rad}} = \frac{16}{3} \sigma T^4 \left(\tau + \frac{4}{3} + \frac{2}{3\tau} \right)^{-1}, \quad (9)$$

where S is the specific entropy, γ is the ratio of specific heat, $c_{\text{s}} = (P/\rho)^{1/2}$ is the sound speed, and $\tau = \kappa \rho H$ is the optical depth, for which the electron scattering is included as the main opacity source, $\kappa = \kappa_{\text{es}} = 0.4$. The quantity Q_{w} in Equation (6) represents the energy carried away by the outflow, which can be expressed by

$$Q_{\text{w}} = 2\eta \left(\frac{1}{2} \dot{m}_{\text{w}} V_{\text{K}}^2 \right), \quad (10)$$

where a factor of 2 signifies the outflow that is emitted bilaterally from the accretion disk, η is a specific energy parameter to determine the outflow strength, and V_{K} is the Keplerian velocity.

Due to the presence of the disk wind, the mass inflow rate would reduce inward. Numerical simulations show that the reduction roughly follows a power law within R_{tr} (e.g. Yang et al. 2014; Kitaki et al. 2021; Yoshioka et al. 2022; Yang et al. 2023), so we take the mass inflow rate varying with radius as (Blandford & Begelman 1999):

$$\dot{M} = -2\pi R \Sigma V_{\text{R}} = \dot{M}_{\text{o}} \left(\frac{R}{R_{\text{o}}} \right)^s, \quad (11)$$

for a disk with $R_{\text{o}} < R_{\text{tr}}$, where \dot{M}_{o} is the mass accretion rate at the disk outer boundary R_{o} , and the power-law index s is a free parameter, constrained within $0 \leq s \leq 1$, which approaches zero in the absence of wind, leading to the disk satisfying the slim solution (e.g. Abramowicz et al. 1988; Narayan & Yi 1995; Watarai & Fukue 1999). Assuming that the complete reduction of mass inflow rate is solely attributed to the disk wind, then, from Equation (2) and (11), we can get

$$\dot{m}_{\text{w}} = \frac{s\dot{M}}{4\pi R^2}. \quad (12)$$

2.2. Self-similar solutions

Although numerical simulations are the more reliable approach for investigating the complicated super-Eddington accretion process around compact objects (e.g. Ohsuga et al. 2005; Jiang et al. 2014; Sądowski et al. 2015; Kitaki et al. 2018; Takahashi et al. 2018; Abarca et al. 2018; Hu et al. 2022), analytic solutions are valuable, as they can roughly match the structure of the accretion systems observed in simulations (e.g. Jiao et al. 2015). Moreover, these

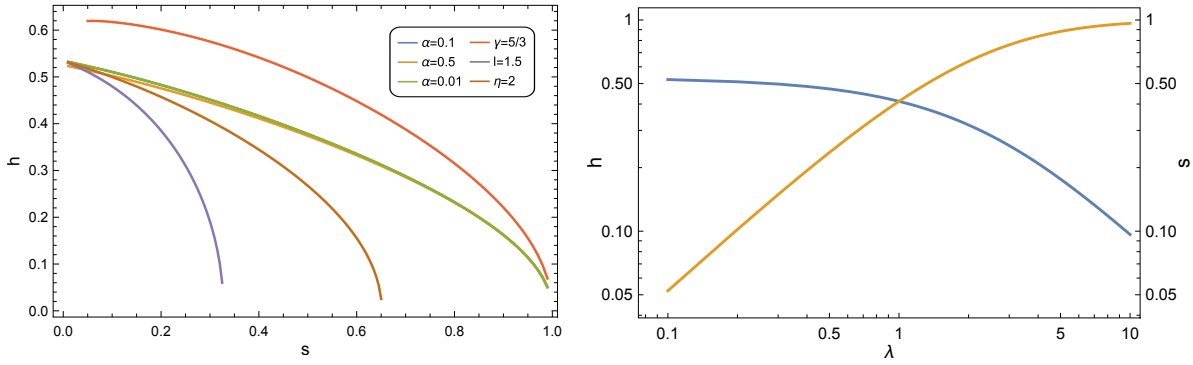


Figure 2. Properties of a super-Eddington accretion disk under self-similar solutions. The left panel represents the disk thickness $h = H/R$ as a function of the inflow power-law index s considering various system parameters (as shown in the inset), where the fiducial ones are $\alpha = 0.1$, $\gamma = 4/3$, $l = 1$, and $\eta = 1$. The right panel shows the variation of h and s as a function of λ , where $\lambda = s/(H/R)$ qualitatively reflects the impact of advection on the disk.

solutions offer convenience in directly constructing circum-CO disks under varying system parameters (e.g. Blandford & Begelman 1999; Begelman 2012; Gu 2015; Ghoreysi & Shadmehri 2020; Zahra Zeraatgari et al. 2020). Because a super-Eddington accretion disk is radiation-ineffective, the radiation cooling term is of minor significance in Equation (6) (e.g. Wu et al. 2022). If we ignore Q_{rad} , a set of self-similar variables— $\rho_s \propto R^{s-3/2}$, $P_s \propto R^{s-5/2}$, $V_{R,s} \propto R^{-1/2}$, $H_s \propto R$, and $\Omega_s \propto r^{-3/2}$ —can simultaneously satisfy the disk Equations (2), (4), (5), and (6). Considering the vertical force balance, the disk height can be expressed as $H = c_s/\Omega_K$ (e.g. Kato et al. 2008). By combining these five equations, a solution to the disk structure can be obtained.

The self-similar solution is:

$$\rho_s = \frac{(1 + 2s - 2l^2s) \dot{M}_o \omega}{4\pi (1 + 2s) \alpha (GM)^{1/2} R_o^{3/2} h^3} \left(\frac{R}{R_o} \right)^{s-3/2}, \quad (13)$$

$$P_s = \frac{(1 + 2s - 2l^2s) \dot{M}_o (GM)^{1/2} \omega}{4\pi (1 + 2s) \alpha R_o^{5/2} h} \left(\frac{R}{R_o} \right)^{s-5/2}, \quad (14)$$

$$V_{R,s} = -\frac{(1 + 2s) \alpha (GM)^{1/2} h^2}{(1 + 2s - 2l^2s) \omega R_o^{1/2}} \left(\frac{R}{R_o} \right)^{-1/2}, \quad (15)$$

$$H_s = hR, \quad (16)$$

$$\Omega_s = \omega \frac{(GM)^{1/2}}{R_o^{3/2}} \left(\frac{R}{R_o} \right)^{-3/2}, \quad (17)$$

where

$$\omega = \frac{1}{2} \left\{ (2s - 5) h^2 + \left[\left((5 - 2s)^2 - \frac{8\alpha(1 + 2s^2)}{1 + 2s - 2l^2s} \right) h^4 + 4(2s - 5) h^2 + 4 \right]^{1/2} + 2 \right\}^{1/2}, \quad (18)$$

and h is solved numerically via Equation (6), i.e.,

$$\frac{3(1 + 2s - 2l^2s)}{4(1 + 2s)} \left\{ (2s - 5) h^2 + \left[(2 + (2s - 5) h^2)^2 - \frac{8(2s + 1)^2 \alpha^2 h^4}{(1 + 2s - 2l^2s)^2} \right]^{1/2} + 2 \right\} + \left(3 - 2s - \frac{2}{\gamma - 1} \right) h^2 - \eta s = 0. \quad (19)$$

As indicated by Equations (13)-(17), the disk properties are influenced by s , α , γ , l , and η . To investigate these dependencies, we take h as an indicator and explore its variation, which is shown in the left panel of Figure 2. First, the super-Eddington accretion disk is geometrically thick, with $h > 0.1$. The value of h decreases with the increase of s , which can be attributed to the enhanced mass loss resulting from a larger s . Consequently, more energy is carried away by the disk wind, leading to a reduction in the thickness of the resultant disk. Second, for a large value of l or η ,

the maximum value of s in a valid solution is less than 1, since a disk would not exist if the loss of angular momentum or energy via the disk wind were to exceed its total reserve. Third, the disk structures are basically not influenced by α , but exhibit sensitivity to γ . In the subsequent calculations, we set $\alpha = 0.1$, $\gamma = 4/3$, $l = 1$, and $\eta = 1$.

Moreover, the selection of s should be based on the disk properties rather than being chosen randomly. Wu et al. (2022) adopt a reasonably appropriate assumption that s is proportional to H/R , i.e., $s = \lambda(H/R)$, where λ is a constant, considering that the disk thickness can reflect the strength of advection. Still, λ is uncertain, but it can be adjusted to encompass all values of s , as shown in the right panel of Figure 2. Therefore, we apply all physical values for s from 0 to 1 to investigate the comprehensive properties of the super-Eddington accretion disk.

3. SUPER-EDDINGTON DISK ACCRETION OF MAGNETIZED NS

The fundamental framework of disk accretion around a magnetized NS is widely accepted in theory works (e.g. Pringle & Rees 1972; Lamb et al. 1973, and see Lai 2014 for a review) and supported by numerical simulations (e.g. Romanova et al. 2004, 2012; Zhu et al. 2024). According to this framework, the circum-NS disk is disrupted by the NS magnetic field due to the high pressure and stress it exerts at the magnetosphere truncation radius. Subsequently, within an interaction boundary layer, the angular velocity of the inflow transitions from the disk value to the NS spin rate through magnetic torque. The gas, coupled with the rotating NS, is then loaded onto closed field lines and funneled to the magnetic poles. Using the disk structures constructed in the previous section, we investigate the specific properties of super-Eddington accretion around the magnetized NS.

3.1. Magnetosphere Truncation Radius

The external magnetic field of an NS exhibits a complex structure superposed by various multipoles (e.g. Bilous et al. 2019). Since the n -th multipole field varies as $B_n \sim \mu_n/R^{n+2}$, where μ_n is the n -th magnetic moment, in regions far from the NS surface, higher multipoles fall off rapidly and the dipole dominates the overall field structure¹. Therefore, at the magnetosphere truncation radius, we adopt a dipole structure for the NS magnetic field with a field strength of $B_0 = \mu/R^3$, where $\mu = 10^{30} \text{ G cm}^3$ is set. Simulations indicate that the formation of a funnel stream occurs approximately at the radius where magnetic and disk pressure reach an equilibrium (Kulkarni & Romanova 2013; Takahashi & Ohsuga 2017). As the inflow mass rate of a super-Eddington disk exhibits radial variation, we employ pressure balance as the criterion for determining the magnetosphere truncation radius R_M ², at which the disk gas becomes trapped by field lines and the mass rate accreted onto the NS is then $\dot{M}_o(R_M/R_o)^s$, i.e.:

$$P_{B0} = P_s, \quad \frac{\mu^2}{8\pi R_M^6} = \frac{(1 + 2s - 2l^2s) \dot{M}_o (GM)^{1/2} \omega}{4\pi (1 + 2s) \alpha R_o^{5/2} h} \left(\frac{R}{R_o} \right)^{s-5/2}, \quad (20)$$

which leads to

$$R_M = k \left(\frac{\mu^4 R_o^{2s}}{GM \dot{M}_o^2} \right)^{1/(7+2s)}, \quad (21)$$

where

$$k = \left[\frac{(1 + 2s) \alpha h}{2(1 + 2s - 2l^2s) \omega} \right]^{2/(7+2s)} \quad (22)$$

describes the dependence of the magnetosphere truncation radius on the properties of a super-Eddington accretion disk. More precisely, the truncation is directly determined by the interaction between the NS magnetosphere and the innermost region of the disk, therefore we also present R_M in a widely accepted form (e.g. Ghosh & Lamb 1979a,b):

$$R_M = k_{\text{in}} \left(\frac{\mu^4}{GM \dot{M}_{\text{in}}^2} \right)^{1/7}, \quad (23)$$

¹ The dipole magnetosphere truncation radius $R_M = 3.9 \times 10^7 \text{ cm } k_{\text{in}} (\mu/10^{30} \text{ G cm}^3)^{4/7} (M/1.4M_\odot)^{-1/7} (\dot{M}_{\text{in}}/10^3 \dot{M}_{\text{Edd}})^{-2/7}$ is much larger than the NS radius, so the multipoles are dominant only if $\mu_n \gg \mu_{\text{dipole}}$. However, near the NS surface, the multipole fields can be comparable or stronger than the dipole component. So, the magnetic field at the NS surface exhibits a complex structure due to the superposition of multipoles with varying tilt angles, guiding the funneled inflow to a area wider than the pure dipole magnetic poles (e.g. Long et al. 2007, 2008; Gregory & Donati 2011). Consequently, the accretion streams would overlap and heat various surface regions of the NS, thereby generating anomalous multiwavelength radiation facilitated by the NS rotation (e.g. Bilous et al. 2019). Additionally, in the case of super-Eddington accretion, the funneled streams can form an optically thick envelope that can then reprocess the photons emitted by the multipole accretion flows encircled in the closed dipole fields, resulting in a more intricate radiation profile (Mushtukov et al. 2019).

² The ram pressure of the accreting gas is negligible compared to the thermal pressure of the disk, as $\rho_s V_{R,s}^2 / P_s = [(1 + 2s) \alpha h / (1 + 2s - 2l^2s) \omega]^2$ is much less than 1, except in the case where $\alpha \sim 1$ with $s \sim 0$. Therefore, we disregard the contribution of this term to the pressure balance at R_M .

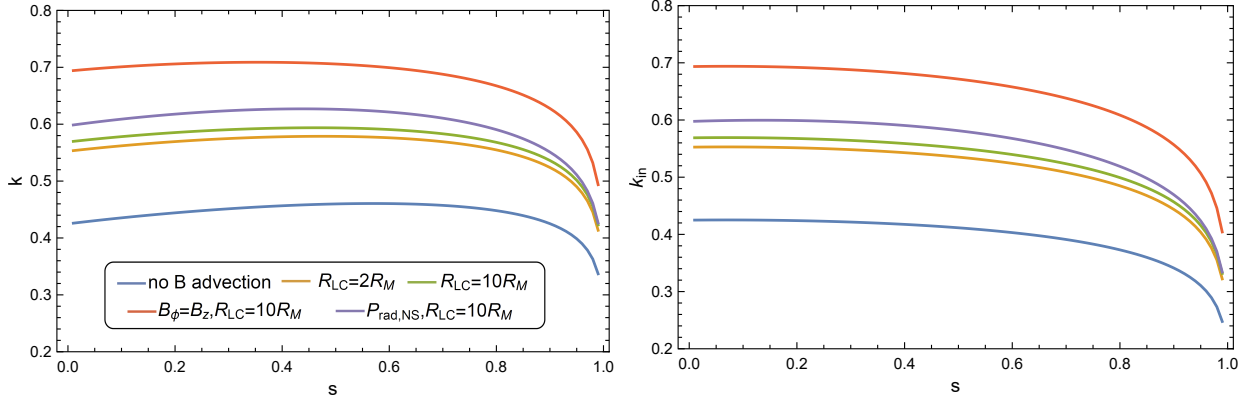


Figure 3. Variation of magnetosphere truncation radius as a function of the super-Eddington accretion disk’s index s , where k and k_{in} are given by Equation (22) and (24), respectively. In each panel, the blue line shows the closed NS magnetic field lines initially threading the disk are inefficiently advected inward with the inflow, while the disk truncation results from the local pressure balance, i.e., $P_{\text{B}0} = P_{\text{s}}$; the golden line shows these closed lines are concentrated at the magnetospheric boundary to enhance the magnetic field strength, with the NS rotating at an angular velocity with $R_{\text{LC}} = 2R_{\text{M}}$, while the green line correspondingly shows the case of a rotating NS with $R_{\text{LC}} = 10R_{\text{M}}$; the orange line shows the compressed dipole lines are strongly twisted to produce a toroidal component with $B_{\phi} = B_z$, which provides extra magnetic pressure; and the purple line considers the extra feedback of the radiation released near the NS on the interaction boundary layer.

where the second factor on the right-hand side is the conventional expression for the magnetosphere radius in the NS spherical accretion system (e.g. [Elsner & Lamb 1977](#)), i.e., the Alfvén radius, with $\dot{M}_{\text{in}} = \dot{M}(R_{\text{M}})$ and

$$k_{\text{in}} = \left[\frac{(1+2s)\alpha h}{2(1+2s-2l^2s)\omega} \right]^{2/7}. \quad (24)$$

To investigate the impact of the super-Eddington flow on the magnetized NS accretion, we examine the correlation between k or k_{in} and s to assess if it deviates significantly from the typical value $k_{\text{in}} \sim 0.4 - 0.8$ (e.g. [Long et al. 2005](#); [Bessolaz et al. 2008](#); [Kulkarni & Romanova 2013](#); [Zanni & Ferreira 2013](#)). As shown in Figure 3, the value of k ranges from 0.34 to 0.46, which is similar but relatively low compared to the typical value, owing to the high pressure of the super-Eddington disk resulting from significant energy storage and advection processes. Furthermore, the variation trend of k on s shows an initial increase followed by a subsequent decrease, which mirrors the behavior of the disk pressure (not depicted in the paper, for conciseness). Notably, k exhibits minimal variation with the change in s , except for $s > 0.9$, where a substantial compression of the NS magnetosphere caused by high P_{s} leads to a reduction of k . Correspondingly, k_{in} varies with the range of 0.25 – 0.43, which is slightly lower than k . Moreover, taking \dot{M}_{in} into account, k_{in} exhibits a monotonic decrease as the value of s increases.

When the NS closed magnetic field lines thread the accretion disk, they simultaneously undergo inward advection, along with inflow and outward diffusion controlled by turbulence (e.g. [Parfrey et al. 2017](#)). The advection of the magnetic field relies on the disk radial velocity $V_{\text{R},s}$, i.e., Equation (15), while its diffusion is determined by the magnetic diffusivity η . In magnetorotational-instability-generated turbulence, η can be expressed as $\eta = \nu/Pr_{\text{m}}$, where $\nu = 2\alpha c_{\text{s}}H/3\omega$ and the magnetic Prandtl number $Pr_{\text{m}} \sim 1$ (e.g. [Lesur & Longaretti 2009](#); [Guan & Gammie 2009](#); [Fromang & Stone 2009](#)), while the resulting diffusion velocity can be approximated as $V_{\text{diff}} \sim \eta/H$ (e.g. [Lubow et al. 1994](#); [Cao 2011](#)). For a super-Eddington accretion disk, using a self-similar solution, we find that $V_{\text{R},s} \gtrsim V_{\text{diff}}$, owing to an effective disk advection. Additionally, as the wind extracts extra angular momentum from the disk, it would lead to Pr_{m} exceeding unity ([Parfrey et al. 2017](#)). Consequently, the threading magnetic field is expected to overcome diffusion and flow inside. To estimate the impact of the field advection, we consider an ideal scenario where all closed magnetic field lines originating from the NS and initially penetrating the accretion disk are advected inward and concentrated at the magnetosphere-disk interaction layer. Adopting the magnetic flux conservation

$$\delta(B \times \text{Area}) = 0, \quad \delta B \pi R^2 + \frac{\mu}{R^3} (-2\pi R \delta R) = 0, \quad (25)$$

the compressed magnetic fields can be derived as

$$\Delta B = \int_R^{R_{\text{LC}}} \delta B = \int_R^{R_{\text{LC}}} \frac{2\mu}{R^4} dR = \frac{2}{3}\mu \left(\frac{1}{R^3} - \frac{1}{R_{\text{LC}}^3} \right), \quad (26)$$

where R_{LC} is the light cylinder radius, inside which the initial NS magnetic field lines are closed. Therefore, the magnetic field at the magnetosphere truncation radius can be estimated by superimposing the compressed component onto the initial value, i.e.:

$$B = B_0 + \Delta B = \frac{\mu}{R^3} \left(\frac{5}{3} - \frac{2}{3} \frac{R^3}{R_{\text{LC}}^3} \right). \quad (27)$$

Due to the concentration of the magnetic field, a higher magnetic pressure, $P_B = B^2/8\pi$, is generated, which pushes the disk outward, consequently resulting in an enlarged magnetosphere truncation radius. Two instances of a rotating NS with $R_{\text{LC}} = 2R_M$ and $R_{\text{LC}} = 10R_M$ are illustrated in Figure 3, the corresponding values of k are raised to 0.41–0.58 and 0.42–0.59, respectively. The similarity between the two values suggests that k or k_{in} is not significantly affected by the NS rotation, which is consistent with Equation (27), where the second term, $\propto R_{\text{LC}}^{-3}$, remains negligible unless the NS rotates very fast, so that $R_{\text{LC}} \sim R_M$. The compressed magnetic field asymptotically approaches $B \simeq 5/3B_0$.

Besides advection and diffusion, the field lines linking the NS and the disk are twisted due to the differential rotation at each end of the footpoints, resulting in the generation of a toroidal field component. The resultant magnetic pressure drives field inflation and reconnection, opening the closed lines to sever the NS-disk linkage, ultimately arresting the growth of the toroidal field (Aly & Kuijpers 1990; Lovelace et al. 1995; Parfrey et al. 2016). Lai (2014) argues that the maximum toroidal twist is $|B_\phi/B_z|_{\text{max}} \sim 1$. By assuming $B_\phi = B_z$, the total magnetic pressure at the magnetosphere-disk interaction layer increases to $B^2/4\pi$, leading to a larger truncation radius. As shown in Figure 3, the resulting values of k and k_{in} are 0.49–0.71 and 0.40–0.69, respectively, which are consistent with the typical values and agree with the simulation results (e.g. Takahashi & Ohsuga 2017), wherein $k_{\text{in}} \sim 0.7$. However, our findings slightly deviate from those of Chashkina et al. (2017, 2019), where the relative magnetosphere radius, i.e., k and k_{in} , exhibits a significant dependence on the inner disk mass inflow rate. We attribute this discrepancy primarily to the differences in the boundary conditions employed. It is worth noting that despite the high efficiency of advection, not all closed magnetic field lines initially threading the accretion disk are swept inward because of magnetic inflation, flux opening, and reconnection (Parfrey et al. 2017). The disk winds also exert a notable impact on the magnetic field structure. Moreover, reconnection prevents the twisted toroidal magnetic field from always remaining at its maximum strength. Therefore, the actual values of k and k_{in} should be lower than those derived from the ideal conditions.

Additionally, when the super-Eddington accretion flow is funneled close to the NS magnetic pole, it gives rise to the formation of an accretion column (Mushtukov et al. 2015a), within which the released gas energy is converted to radiation and subsequently escapes from its lateral surface (e.g. Mushtukov et al. 2015b; Kawashima et al. 2016; Mushtukov et al. 2018). When these photons from the NS illuminate the interaction boundary, an extra radiation pressure is exerted upon it (e.g. Chashkina et al. 2019). Considering this pressure component, the equilibrium criterion is modified to

$$P_B + P_{\text{rad,NS}} = P_s, \quad P_{\text{rad,NS}} = \frac{L_{\text{rad,NS}}}{4\pi R_M^2 c}, \quad (28)$$

where $L_{\text{rad,NS}} \simeq GM\dot{M}_{\text{in}}/R_{\text{NS}}$ is the luminosity of the radiation emitted from the accretion column, $R_{\text{NS}} = 10^6$ cm represents the NS radius, and the radiation is simplified to be isotropic. The value of k and k_{in} for a case of contrast, as shown in Figure 3, ranges between 0.43–0.63 and 0.34–0.60, respectively. These values are slightly higher than those obtained when disregarding the contribution of the accretion column radiation, yet the deviation remains within 5%, suggesting that the impact of this radiation effect on disk truncation is insignificant.

In brief, the magnetosphere truncation radius, which is influenced by the properties of the super-Eddington disk and determines the mass accretion rate onto the NS, is found to be proportional to the Alfvén radius, as described by Equations (22) and (24), where k and k_{in} vary within the ranges of 0.34–0.71 and 0.25–0.69, respectively, depending on various effects, including the advection and twisting of the magnetic field, the rotation of the NS, as well as the radiation emitted from the NS accretion column. The resulting mass rate accreted onto the NS is approximated as $\dot{M}_{\text{in}} = \dot{M}_o (R_M/R_o)^s$.

3.2. Thickness of Interaction Boundary Layer

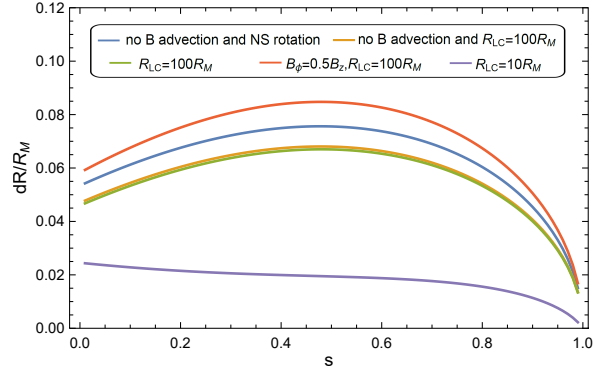


Figure 4. Relative thickness of the magnetosphere-disk interaction boundary layer, i.e., $\Delta R/R_M$, as a function of s for a sample system with $\dot{M}_o = 10^4 \dot{M}_{\text{Edd}}$ and $R_o = 10^4 R_g$. The blue line represents the case of no magnetic field advection within the disk and the NS without spinning, i.e., $R_{\text{LC}} \rightarrow \infty$, while the golden line correspondingly shows the case of $R_{\text{LC}} = 100R_M$; the green line shows that the magnetic fields are concentrated and $R_{\text{LC}} = 100R_M$, the orange line reduces the degree of field twisting to $B_\phi = 0.5B_z$; and the purple line speeds up the NS rotation to $R_{\text{LC}} = 10R_M$. $\Delta R/R_M \ll 1$ always holds, indicating that the boundary layer is very thin.

At the truncation radius, though the NS magnetic pressure hinders the disk inflow, various instabilities can arise to facilitate further plasma penetration into the magnetosphere (Romanova & Owocki 2015 and references therein). The differential rotation between the NS and the magnetosphere plasma causes a twisting of the field lines, in turn resulting in the generation of magnetic torque to eliminate the rotational difference within a boundary layer (e.g. Spruit & Taam 1993; Rappaport et al. 2004; Lai 2014). In the case of a typical Keplerian disk, the interaction boundary layer is thin (e.g. Kulkarni & Romanova 2013; Ćemeljić et al. 2023); for comparative analysis, we explore the thickness of this layer under super-Eddington disk conditions. Taking into account the contribution of both the twisting magnetic field lines above and below the disk midplane, the magnetic torque per unit area can be expressed as $R_M B_\phi B_z / 2\pi$, facilitating the transition of the inflow angular velocity from the disk's Ω_s to the NS spin rate Ω_{NS} within the boundary layer, i.e.:

$$2\pi R_M^2 \Delta R \frac{B_\phi B_z}{2\pi} = R_M^2 \Delta R B_\phi B_z = \dot{M}_{\text{in}} |R_M^2 \Omega_s - (R_M - \Delta R)^2 \Omega_{\text{NS}}|, \quad (29)$$

where ΔR is the layer radial thickness, and the absolute value quantifies the overall change in the inflow's specific angular momentum.

The relative thickness of the interaction boundary layer, $\Delta R/R_M$, under various conditions is shown in Figure 4; in all cases, unless otherwise specified, we assume that the field twisting results in $B_\phi = B_z$. When the NS spin rate is low, or even when the NS is approximately nonrotating, i.e., $\Omega_{\text{NS}} \sim 0$, the second term in the absolute sign of Equation (29) can be neglected, and the layer thickness is reduced to

$$\Delta R = \frac{\dot{M}_{\text{in}} \Omega_s R_M^6}{\mu^2}, \quad (30)$$

which is thin, with a relative thickness smaller than 0.1. The variation trend of $\Delta R/R_M$ on s exhibits a similar pattern to that of R_M or k , initially increasing and then decreasing, attributed to the layer thickness being determined by the torque exerted by the magnetic fields, which is directly influenced by the magnetosphere truncation radius through $B \propto R_M^{-3}$. Spinning up the NS, for example to $R_{\text{LC}} = 100R_M$, diminishes the gap in angular velocity between it and the disk, causing a thinner layer; as a comparison, for an NS with $R_{\text{LC}} = 10R_M$, its angular velocity closely matches that of the disk, leading to an extremely thin boundary. The inclusion of field advection and accumulation leads to a decrease in the relative layer thickness, as a stronger field generates a larger torque; however, this effect is not highly significant. On the contrary, when the degree of field twisting is low, for instance, $B_\phi = 0.5B_z$, the resulting magnetic torque is attenuated; to fully transform the rotation of disk gas, a thicker layer is required, for which the relative thickness still remains below 0.1. Overall, the interaction boundary layer between the NS magnetosphere and the super-Eddington disk is thin, in turn ensuring the availability of Equation (29), as both the NS magnetic field and the mass inflow rate remain relatively constant within a narrow ΔR .

4. DISCUSSION

4.1. Propeller regime

In an NS disk accretion system, when the NS rotates slower than the disk at its inner boundary, after being coupled with the magnetosphere, the braked inflow can no longer counteract gravity and becomes channeled toward the NS magnetic poles along the field lines. Conversely, when the NS is the faster object, the disk gas is accelerated by the magnetic torque to gain angular momentum, and the resulting enhanced centrifugal force hinders the subsequent accretion and may even lead to the ejection of most of the mass at the magnetosphere boundary, forming an outflow; this process is called the propeller regime (e.g. Illarionov & Sunyaev 1975; Lovelace et al. 1999; Ustyugova et al. 2006). By defining a fastness parameter, $\omega_s = \Omega_{\text{NS}}/\Omega_s(R_M)$, the NS is spun up through gas accretion when $\omega_s < 1$ and is spun down by interaction torque when $\omega_s > 1$. Consequently, the NS reaches an equilibrium state approximately at $\omega_s \simeq 1$ (e.g. Long et al. 2005; Dai & Li 2006; Lai 2014) and the corresponding NS spin period is

$$P_{\text{eq}} = \frac{2\pi}{\Omega_s(R_M)} = 2\pi\omega^{-1}k_{\text{in}}^{3/2} (GM)^{-5/7} \left(\frac{\mu^2}{\dot{M}_{\text{in}}}\right)^{3/7} = 0.03 \text{ s} \left(\frac{\mu}{10^{30} \text{ G cm}^3}\right)^{6/7} \left(\frac{M}{1.4M_{\odot}}\right)^{-5/7} \left(\frac{\dot{M}_{\text{in}}}{10^3 \dot{M}_{\text{Edd}}}\right)^{-3/7}, \quad (31)$$

where the constant $2\pi\omega^{-1}k_{\text{in}}^{3/2}$ varies in the range 1 – 3 as a function of s . The timescale for the accretion-induced spinup of an initially nonrotating NS to reach its equilibrium state can be roughly estimated as

$$I\Delta\Omega_{\text{NS}} \simeq \dot{M}_{\text{in}}R_M^2\Omega_s(R_M)\Delta t, \quad (32)$$

where $I \sim MR_{\text{NS}}^2$ is the moment of inertia of the NS, leading to

$$\Delta t \simeq \frac{I}{\dot{M}_{\text{in}}R_M^2} = 1.7 \times 10^3 \text{ yr } k_{\text{in}}^{-2} \left(\frac{\mu}{10^{30} \text{ G cm}^3}\right)^{-8/7} \left(\frac{M}{1.4M_{\odot}}\right)^{9/7} \left(\frac{R_{\text{NS}}}{10 \text{ km}}\right)^2 \left(\frac{\dot{M}_{\text{in}}}{10^3 \dot{M}_{\text{Edd}}}\right)^{-3/7}, \quad (33)$$

within which the accretion process has negligible impact on the mass and radius of the NS. Correspondingly, the NS spinup rate is

$$\frac{2\pi I \dot{P}}{P^2} \simeq \dot{M}_{\text{in}}\sqrt{GMR_M}, \quad \dot{P} = 9.8 \times 10^{-10} \text{ s s}^{-1} k_{\text{in}}^{1/2} \left(\frac{\mu}{10^{30} \text{ G cm}^3}\right)^{2/7} \left(\frac{M}{1.4M_{\odot}}\right)^{-4/7} \left(\frac{R_{\text{NS}}}{10 \text{ km}}\right)^2 \left(\frac{\dot{M}_{\text{in}}}{10^3 \dot{M}_{\text{Edd}}}\right)^{6/7} \left(\frac{P}{1 \text{ s}}\right)^2. \quad (34)$$

Therefore, in the case of super-Eddington accretion, an NS can readily undergo rapid spinup given a high mass accretion rate, as observed in ULXP sources, such as the NGC 5907 ULXP with an X-ray luminosity $\geq 10^{41} \text{ erg s}^{-1}$ (Israel et al. 2017), provided that the luminosity accurately reflects the actual accretion rate³, or within AGN disk environments, where the NS accretion rate can reach $10^5 - 10^6 \dot{M}_{\text{Edd}}$ (e.g. Chen et al. 2023). Moreover, the magnetic field experiences decay throughout the NS accretion process (e.g. Mukherjee 2017; Konar 2017; Igoshev et al. 2021), resulting in a reduction of the equilibrium spin period P_{eq} due to an increased inflow-specific angular velocity at smaller R_M . However, the decrease in inflow angular momentum leads to slower spinup, as indicated by Equation (33) and (34). Besides, through the analysis of ULXPs, one can derive P and \dot{P} while estimating \dot{M}_{in} for the system, thereby establishing a lower limit on the strength of the NS magnetic field. The properties of the super-Eddington disk wind slightly influence the estimation of the NS magnetic field strength, as indicated by Equation (34), where $\mu \propto k_{\text{in}}^{-7/4}$ while k_{in} is not significantly relying on s . But the geometrical beaming originating from the wind leads to an overestimation of \dot{M}_{in} , thus μ is significantly underestimated, since $\mu \propto \dot{M}_{\text{in}}^{-3}$.

4.2. Error from radiation cooling

To construct a self-similar super-Eddington accretion disk, we have neglected the radiation cooling term in Equation (6). In this subsection, we investigate whether Q_{rad} is indeed a small factor that does not significantly impact the

³ Among the $O(10^3)$ observed ULX candidates (Walton et al. 2022), only a few sources exhibit pulsations, providing confirmation of their central object being an NS, as shown in Table 2 of King et al. (2023). Due to the limited number of ULXPs, conducting statistical studies to investigate the general properties of these sources is currently unfeasible. The observed X-ray luminosity of the ULXPs ranging between $10^{39} - 10^{41} \text{ erg s}^{-1}$ indicates a range of the maximum NS accretion rate $10^2 - 10^4 \dot{M}_{\text{Edd}}$. For a strong magnetic field of $\mu \gtrsim 10^{31} \text{ G cm}^3$ (e.g. Chashkina et al. 2019), the equilibrium period is approximately $P_{\text{eq}} \sim 0.08 - 0.58 \text{ s}$, considering the geometrical beaming would decrease \dot{M}_{in} to further raise the period to $O(1) \text{ s}$. Despite $P_{\text{eq}} = O(10^{-2}) \text{ s}$, the lifetime of the NS accreting system in ULX mode remains uncertain (Fabrika et al. 2021), thereby precluding its eventual evolution toward an equilibrium state. The properties of the ULXP systems deserve further investigation.

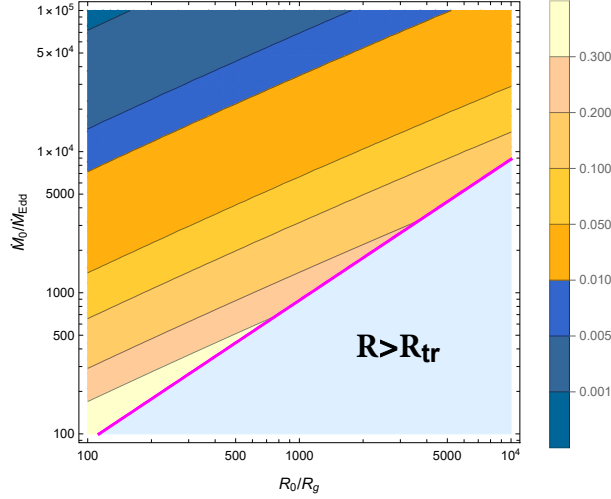


Figure 5. Radiation cooling as a percentage of total disk energy, $Q_{\text{rad}}/(Q_{\text{vis}} + Q_{\text{rad}})$, in the $R_o - \dot{M}_o$ parameter space in the case of $s = 0.5$, where the energy rates are divided from the self-similar solutions, roughly describing the derivation of the solutions ignoring radiation cooling from the real disk. The magenta line and the region to the tight represent the case of $R_o \geq R_{\text{tr}}$, where the disk photons can efficiently diffuse out and the disk wind would fail to launch, therefore the super-Eddington disk solution is invalid and the disk transitions to be geometrically thin.

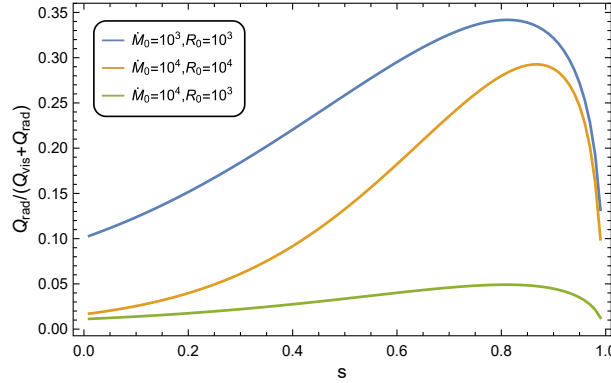


Figure 6. Radiation cooling ratio $Q_{\text{rad}}/(Q_{\text{vis}} + Q_{\text{rad}})$ as a function of s , where three cases are taken as examples: $\dot{M}_o = 10^3 \dot{M}_{\text{Edd}}$ with $R_o = 10^3 R_g$, $\dot{M}_o = 10^4 \dot{M}_{\text{Edd}}$ with $R_o = 10^4 R_g$, and $\dot{M}_o = 10^5 \dot{M}_{\text{Edd}}$ with $R_o = 10^4 R_g$.

disk structure. Roughly speaking, the self-similar disk should produce some additional energy, except its initial Q_{vis} for the runaway radiation. So, using Equation (9), we calculate the radiation cooling that the self-similar disk is supposed to generate and compare it with the total energy of the disk encompassing this energy, i.e., $Q_{\text{vis}} + Q_{\text{rad}}$. Figure 5 and 6 illustrate $Q_{\text{rad}}/(Q_{\text{vis}} + Q_{\text{rad}})$ as a function of $R_o - \dot{M}_o$ and s , respectively. From the figures, the ratio is consistently much less than unity, indicating that radiation cooling would not significantly impact the structure of the super-Eddington disk, except for the case of $R_o \sim R_{\text{tr}}$ yet $\dot{M}_o/\dot{M}_{\text{Edd}} \lesssim 1000$, where the disk size becomes relatively small, hindering efficient photon advection within it. Both increasing \dot{M}_o and decreasing R_o to achieve $R_o \ll R_{\text{tr}}$ can mitigate the impact of radiation cooling, thereby promoting self-similarity in super-Eddington disks; two concrete disk structures are shown in the Appendix A to illustrate this property.

The disk radiation cooling, in addition, does not exert a significant effect on the accretion process of the NS. The magnetosphere truncation radius is directly determined by the disk pressure, which only exhibits a slight deviation from the self-similar value when considering radiation effects, as shown in Figure 7, as R_M . Or, more intuitively, the inclusion of radiation cooling requires an increase of disk inflow mass rate to generate more energy. Given that

Q_{rad} is much lower than Q_{vis} , the alteration in the mass rate would thus be substantially smaller than \dot{M}_o ; since $R_M \propto \dot{M}_o^{2/(7+2s)}$, its relative change can be neglected.

4.3. Caveat

In this paper, we construct the radial structure of the super-Eddington disk and adopt the vertical hydrostatic equilibrium assumption. Although the resulting self-similar solution can conveniently provide the disk properties under given initial conditions, they should be regarded as approximations. In reality, the analytical solution for the disks should incorporate a three-dimensional or at least two-dimensional structure and discard the vertical force balance assumption, as the formation of disk winds indicates the dynamic nature of the vertical gas; only by constructing a stratified disk structure can we better predict the properties of the disk wind and inflow (e.g. Cao & Gu 2022; Jiao 2023).

Besides, when investigating the magnetosphere-disk interaction, the NS magnetic field is simplified as a dipole. However, the presence of an accretion disk would result in the compression of the magnetosphere into a nondipole shape, thereby impacting the disk truncation (e.g. Aly 1980; Kulkarni & Romanova 2013). In addition, accretion onto the NS solid surface introduces radiation feedback, which not only induces an outward displacement of the disk inner boundary, as shown in Figure 3, but also brings about significant alterations to the disk vertical structure (e.g. Takahashi & Ohsuga 2017; Takahashi et al. 2018). Furthermore, the disk wind would interact with the open field lines (e.g. Mushtukov & Portegies Zwart 2023), leading to reciprocal influences on their respective properties, which would thereby alter the magnetic field structure and affect the disk cooling and angular momentum transfer.

In a word, to provide a more precise depiction of the super-Eddington magnetized NS accretion system, it is imperative to construct a two-dimensional disk and explore the intricate interplay among the disk, the NS magnetic field, the disk wind, and the NS radiation, which will be studied elsewhere.

5. SUMMARY

In this work, we have explored the properties of a super-Eddington magnetized NS accretion system. To comprehensively analyze the system, we have developed general self-similar solutions for the disk structure by considering variable properties of the disk wind, including its mass rate, specific energy, and angular momentum. Extending the disk toward the vicinity of the NS, we have investigated the specific interaction between the disk and the NS magnetosphere, finding that the entire accretion process exhibits similar properties to a typical system involving a sub-Eddington Keplerian disk, where the magnetosphere truncation radius is approximately proportional to the Alfvén radius, and the interaction boundary layer is thin. The magnetosphere truncation is slightly influenced by variations in the super-Eddington disk wind, unless the wind exhibits significant strength; conversely, it is predominantly affected by the advection and twisting of the NS magnetic fields. Additionally, the rotation of the NS and the radiation feedback from its accretion column are secondary factors. The resulting proportional coefficient varies within the range of 0.34 – 0.71. Although containing simplification, we suggest that our model can provide a preliminary description of the accretion system, thus serving as a foundation for constructing a more accurate system structure or for studying the evolution of NSs under super-Eddington disk accretion.

¹ This work was supported by the National SKA Program of China (grant No. 2020SKA0120302), and the National
² Natural Science Foundation of China (grant No. 12393812).

APPENDIX

A. NUMERICAL SOLUTIONS OF SUPER-EDDINGTON ACCRETION DISK

To directly demonstrate the impact of neglecting the radiation cooling term in Equation (6) on disk structures, we employ the disk self-similar solutions at the outer radius as boundary conditions and numerically solve differential Equations (2)-(6) inward to determine the resultant disk structure. To specify the property of the disk wind, we adopt $s = \lambda(H/R)$ with $\lambda = 1$, and the obtained value of s is 0.412. Two examples, $\dot{M}_o = 10^3 \dot{M}_{\text{Edd}}$, $R_o = 10^3 R_g$ representing scenarios where $R_o \sim R_{\text{tr}}$, and $\dot{M}_o = 10^4 \dot{M}_{\text{Edd}}$, $R_o = 10^3 R_g$ representing scenarios where $R_o \ll R_{\text{tr}}$, are shown in Figure 7. From the figure, the numerical solution exhibits minimal deviation from the self-similar one

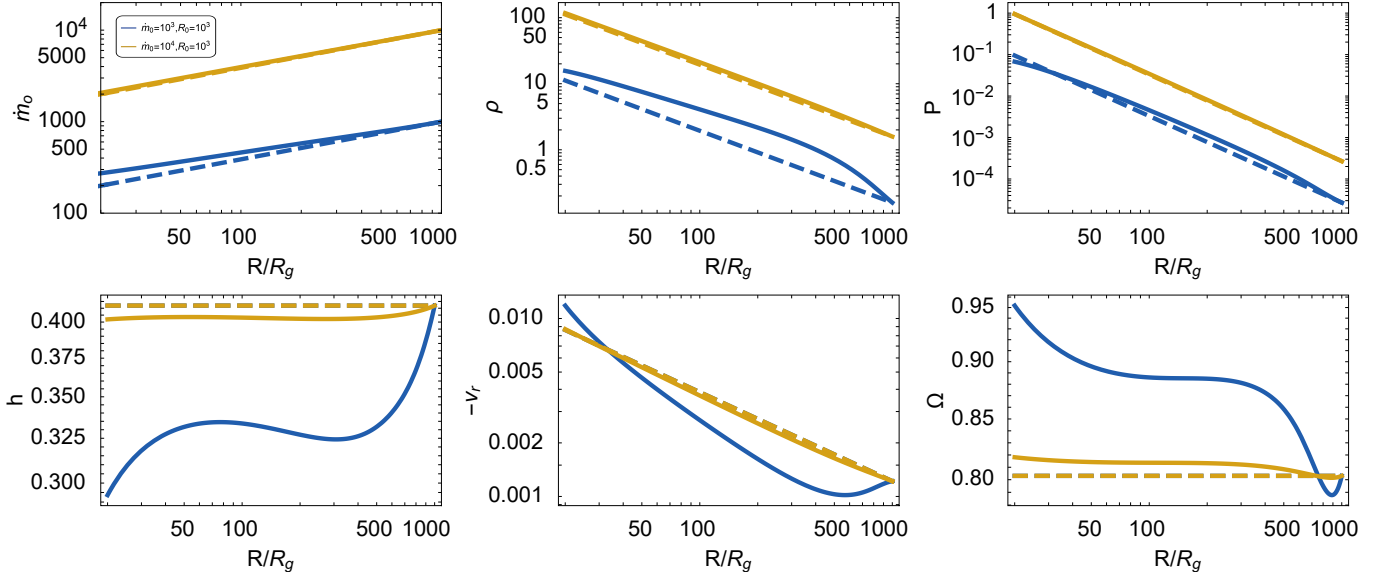


Figure 7. The deviation between numerical and analytic solutions of super-Eddington accretion disks, taking a self-similar solution as the boundary conditions. In each panel, the blue lines show the case of $\dot{M}_o = 10^3 \dot{M}_{\text{Edd}}$, $R_o = 10^3 R_g$, and the golden lines show the case of $\dot{M}_o = 10^4 \dot{M}_{\text{Edd}}$, $R_o = 10^3 R_g$; the dashed lines are the self-similar solutions ignoring radiation cooling, and the solid lines are the structures derived from numerically solving the disk equations directly. All the disk parameters are dimensionless, with \dot{m}_o , ρ , P , h , v_r , and Ω as units of \dot{M}_{Edd} , $\dot{M}_{\text{Edd}}/\sqrt{GM/R_g^3}$, $\dot{M}_{\text{Edd}}\sqrt{GM/R_g^5}$, R_g , $\sqrt{GM/R_g}$, and $\sqrt{GM/R_g^3}$, respectively.

when $R_o \ll R_{\text{tr}}$, as the contribution of the radiation cooling is negligible, which is also illustrated in Figure 6. But when $R_o \sim R_{\text{tr}}$, the proportion of the radiation cooling is increased, resulting in a slight deviation of \dot{m}_o , ρ , and P . Additionally, due to the crucial role of boundary conditions in solving differential equations, selecting the self-similar values for inwardly numerical calculations would lead to an accumulative deviation of h , v_r , and Ω . On the whole, the analytic self-similar solution exhibits a reasonable level of validity, while the numerical solution of a super-Eddington accretion disk deserves further investigation.

REFERENCES

- Abarca, D., Kluźniak, W., & Sądowski, A. 2018, *MNRAS*, 479, 3936. doi:10.1093/mnras/sty1602
- Abarca, D., Parfrey, K., & Kluźniak, W. 2021, *ApJL*, 917, L31. doi:10.3847/2041-8213/ac1859
- Abolmasov, P., Biryukov, A., & Popov, S. B. 2024, *Galaxies*, 12, 7. doi:10.3390/galaxies12010007
- Abramowicz, M. A., Czerny, B., Lasota, J. P., et al. 1988, *ApJ*, 332, 646. doi:10.1086/166683
- Abramowicz, M. A., Chen, X., Kato, S., et al. 1995, *ApJL*, 438, L37. doi:10.1086/187709
- Aly, J. J. 1980, *A&A*, 86, 192
- Aly, J. J. & Kuijpers, J. 1990, *A&A*, 227, 473
- Ascenzi, S., Graber, V., & Rea, N. 2024, *Astroparticle Physics*, 158, 102935. doi:10.1016/j.astropartphys.2024.102935
- Begelman, M. C. 2012, *MNRAS*, 420, 2912. doi:10.1111/j.1365-2966.2011.20071.x
- Bessolaz, N., Zanni, C., Ferreira, J., et al. 2008, *A&A*, 478, 155. doi:10.1051/0004-6361:20078328
- Bhattacharya, D. & van den Heuvel, E. P. J. 1991, *PhR*, 203, 1. doi:10.1016/0370-1573(91)90064-S
- Bilous, A. V., Watts, A. L., Harding, A. K., et al. 2019, *ApJL*, 887, L23. doi:10.3847/2041-8213/ab53e7
- Blandford, R. D. & Begelman, M. C. 1999, *MNRAS*, 303, L1. doi:10.1046/j.1365-8711.1999.02358.x
- Bozzo, E., Falanga, M., & Stella, L. 2008, *ApJ*, 683, 1031. doi:10.1086/589990
- Cao, X. 2011, *ApJ*, 737, 94. doi:10.1088/0004-637X/737/2/94
- Cao, X. & Gu, W.-M. 2022, *ApJ*, 936, 141. doi:10.3847/1538-4357/ac8980
- Čemeljić, M., Kluźniak, W., & Parthasarathy, V. 2023, *A&A*, 678, A57. doi:10.1051/0004-6361/202140637

- Chashkina, A., Abolmasov, P., & Poutanen, J. 2017, *MNRAS*, 470, 2799. doi:10.1093/mnras/stx1372
- Chashkina, A., Lipunova, G., Abolmasov, P., et al. 2019, *A&A*, 626, A18. doi:10.1051/0004-6361/201834414
- Chen, K., Ren, J., & Dai, Z.-G. 2023, *ApJ*, 948, 136. doi:10.3847/1538-4357/acc45f
- Chevalier, R. A. 1989, *ApJ*, 346, 847. doi:10.1086/168066
- Dai, H.-L. & Li, X.-D. 2006, *A&A*, 451, 581. doi:10.1051/0004-6361:20053907
- Elsner, R. F. & Lamb, F. K. 1977, *ApJ*, 215, 897. doi:10.1086/155427
- Fabrika, S. N., Atapin, K. E., Vinokurov, A. S., et al. 2021, *Astrophysical Bulletin*, 76, 6. doi:10.1134/S1990341321010077
- Fornasini, F. M., Antoniou, V., & Dubus, G. 2023, arXiv:2308.02645. doi:10.48550/arXiv.2308.02645
- Fromang, S. & Stone, J. M. 2009, *A&A*, 507, 19. doi:10.1051/0004-6361/200912752
- Gregory, S. G. & Donati, J.-F. 2011, *Astronomische Nachrichten*, 332, 1027. doi:10.1002/asna.201111621
- Ghoreyshi, S. M. & Shadmehri, M. 2020, *MNRAS*, 493, 5107. doi:10.1093/mnras/staa599
- Ghosh, P. & Lamb, F. K. 1979, *ApJ*, 232, 259. doi:10.1086/157285
- Ghosh, P. & Lamb, F. K. 1979, *ApJ*, 234, 296. doi:10.1086/157498
- Gu, W.-M. 2015, *ApJ*, 799, 71. doi:10.1088/0004-637X/799/1/71
- Guan, X. & Gammie, C. F. 2009, *ApJ*, 697, 1901. doi:10.1088/0004-637X/697/2/1901
- Harding, A. K. 2013, *Frontiers of Physics*, 8, 679. doi:10.1007/s11467-013-0285-0
- Hu, H., Inayoshi, K., Haiman, Z., et al. 2022, *ApJ*, 934, 132. doi:10.3847/1538-4357/ac75d8
- Igoshev, A. P., Popov, S. B., & Hollerbach, R. 2021, *Universe*, 7, 351. doi:10.3390/universe7090351
- Illarionov, A. F. & Sunyaev, R. A. 1975, *A&A*, 39, 185
- Inoue, A., Ohsuga, K., Takahashi, H. R., et al. 2023, *ApJ*, 952, 62. doi:10.3847/1538-4357/acd6ea
- Israel, G. L., Belfiore, A., Stella, L., et al. 2017, *Science*, 355, 817. doi:10.1126/science.aai8635
- Jiang, Y.-F., Stone, J. M., & Davis, S. W. 2014, *ApJ*, 796, 106. doi:10.1088/0004-637X/796/2/106
- Jiao, C.-L., Mineshige, S., Takeuchi, S., et al. 2015, *ApJ*, 806, 93. doi:10.1088/0004-637X/806/1/93
- Jiao, C.-L. 2023, *ApJ*, 955, 20. doi:10.3847/1538-4357/aceaf5
- Kawashima, T., Mineshige, S., Ohsuga, K., et al. 2016, *PASJ*, 68, 83. doi:10.1093/pasj/psw075
- King, A., Lasota, J.-P., & Middleton, M. 2023, *NewAR*, 96, 101672. doi:10.1016/j.newar.2022.101672
- Kitaki, T., Mineshige, S., Ohsuga, K., et al. 2018, *PASJ*, 70, 108. doi:10.1093/pasj/psy110
- Kitaki, T., Mineshige, S., Ohsuga, K., et al. 2021, *PASJ*, 73, 450. doi:10.1093/pasj/psab011
- Knigge, C. 1999, *MNRAS*, 309, 409. doi:10.1046/j.1365-8711.1999.02839.x
- Konar, S. 2017, *Journal of Astrophysics and Astronomy*, 38, 47. doi:10.1007/s12036-017-9467-4
- Kulkarni, A. K. & Romanova, M. M. 2013, *MNRAS*, 433, 3048. doi:10.1093/mnras/stt945
- Lai, D. 2014, *European Physical Journal Web of Conferences*, 64, 01001. doi:10.1051/epjconf/20136401001
- Lamb, F. K., Pethick, C. J., & Pines, D. 1973, *ApJ*, 184, 271. doi:10.1086/152325
- Lasota, J.-P. & King, A. 2023, *MNRAS*, 526, 2506. doi:10.1093/mnras/stad2926
- Lesur, G. & Longaretti, P.-Y. 2009, *A&A*, 504, 309. doi:10.1051/0004-6361/200912272
- Long, M., Romanova, M. M., & Lovelace, R. V. E. 2005, *ApJ*, 634, 1214. doi:10.1086/497000
- Long, M., Romanova, M. M., & Lovelace, R. V. E. 2007, *MNRAS*, 374, 436. doi:10.1111/j.1365-2966.2006.11192.x
- Long, M., Romanova, M. M., & Lovelace, R. V. E. 2008, *MNRAS*, 386, 1274. doi:10.1111/j.1365-2966.2008.13124.x
- Lovelace, R. V. E., Romanova, M. M., & Bisnovatyi-Kogan, G. S. 1995, *MNRAS*, 275, 244. doi:10.1093/mnras/275.2.244
- Lovelace, R. V. E., Romanova, M. M., & Bisnovatyi-Kogan, G. S. 1999, *ApJ*, 514, 368. doi:10.1086/306945
- Lubow, S. H., Papaloizou, J. C. B., & Pringle, J. E. 1994, *MNRAS*, 267, 235. doi:10.1093/mnras/267.2.235
- McKernan, B., Ford, K. E. S., & O'Shaughnessy, R. 2020, *MNRAS*, 498, 4088. doi:10.1093/mnras/staa2681
- Mukherjee, D. 2017, *Journal of Astrophysics and Astronomy*, 38, 48. doi:10.1007/s12036-017-9465-6
- Mushtukov, A. A., Suleimanov, V. F., Tsygankov, S. S., et al. 2015, *MNRAS*, 447, 1847. doi:10.1093/mnras/stu2484
- Mushtukov, A. A., Suleimanov, V. F., Tsygankov, S. S., et al. 2015, *MNRAS*, 454, 2539. doi:10.1093/mnras/stv2087
- Mushtukov, A. A., Tsygankov, S. S., Suleimanov, V. F., et al. 2018, *MNRAS*, 476, 2867. doi:10.1093/mnras/sty379
- Mushtukov, A. A., Ingram, A., Middleton, M., et al. 2019, *MNRAS*, 484, 687. doi:10.1093/mnras/sty3525
- Mushtukov, A. & Tsygankov, S. 2022, arXiv:2204.14185. doi:10.48550/arXiv.2204.14185
- Mushtukov, A. A. & Portegies Zwart, S. 2023, *MNRAS*, 518, 5457. doi:10.1093/mnras/stac3431

- Narayan, R. & Yi, I. 1995, *ApJ*, 452, 710.
doi:10.1086/176343
- Ohsuga, K., Mori, M., Nakamoto, T., et al. 2005, *ApJ*, 628, 368. doi:10.1086/430728
- Ohsuga, K. & Mineshige, S. 2007, *ApJ*, 670, 1283.
doi:10.1086/522324
- Ohsuga, K. 2007, *PASJ*, 59, 1033.
doi:10.1093/pasj/59.5.1033
- Pan, Z. & Yang, H. 2021, *ApJ*, 923, 173.
doi:10.3847/1538-4357/ac249c
- Parfrey, K., Spitkovsky, A., & Beloborodov, A. M. 2016, *ApJ*, 822, 33. doi:10.3847/0004-637X/822/1/33
- Parfrey, K., Spitkovsky, A., & Beloborodov, A. M. 2017, *MNRAS*, 469, 3656. doi:10.1093/mnras/stx950
- Perna, R., Tagawa, H., Haiman, Z., et al. 2021, *ApJ*, 915, 10. doi:10.3847/1538-4357/abfdb4
- Pringle, J. E. & Rees, M. J. 1972, *A&A*, 21, 1
- Proga, D. 2000, *ApJ*, 538, 684. doi:10.1086/309154
- Rappaport, S. A., Fregeau, J. M., & Spruit, H. 2004, *ApJ*, 606, 436. doi:10.1086/382863
- Reig, P. 2011, *Ap&SS*, 332, 1.
doi:10.1007/s10509-010-0575-8
- Romanova, M. M., Ustyugova, G. V., Koldoba, A. V., et al. 2004, *ApJ*, 610, 920. doi:10.1086/421867
- Romanova, M. M., Ustyugova, G. V., Koldoba, A. V., et al. 2012, *MNRAS*, 421, 63.
doi:10.1111/j.1365-2966.2011.20055.x
- Romanova, M. M. & Owocki, S. P. 2015, *SSRv*, 191, 339.
doi:10.1007/s11214-015-0200-9
- Sądowski, A., Narayan, R., Tchekhovskoy, A., et al. 2015, *MNRAS*, 447, 49. doi:10.1093/mnras/stu2387
- Shakura, N. I. & Sunyaev, R. A. 1973, *A&A*, 24, 337
- Shakura, N. & Postnov, K. 2017, arXiv:1702.03393.
doi:10.48550/arXiv.1702.03393
- Sirko, E. & Goodman, J. 2003, *MNRAS*, 341, 501.
doi:10.1046/j.1365-8711.2003.06431.x
- Spruit, H. C. & Taam, R. E. 1993, *ApJ*, 402, 593.
doi:10.1086/172162
- Tagawa, H., Kocsis, B., Haiman, Z., et al. 2021, *ApJ*, 908, 194. doi:10.3847/1538-4357/abd555
- Takahashi, H. R. & Ohsuga, K. 2017, *ApJL*, 845, L9.
doi:10.3847/2041-8213/aa8222
- Takahashi, H. R., Mineshige, S., & Ohsuga, K. 2018, *ApJ*, 853, 45. doi:10.3847/1538-4357/aaa082
- Kato, S., Fukue, J., & Mineshige, S. 2008, *Black-Hole Accretion Disks — Towards a New Paradigm —*, 549 pages, including 12 Chapters, 9 Appendices, ISBN 978-4-87698-740-5, Kyoto University Press (Kyoto, Japan), 2008.
- Ustyugova, G. V., Koldoba, A. V., Romanova, M. M., et al. 2006, *ApJ*, 646, 304. doi:10.1086/503379
- Walton, D. J., Mackenzie, A. D. A., Gully, H., et al. 2022, *MNRAS*, 509, 1587. doi:10.1093/mnras/stab3001
- Watarai, K.-. ya . & Fukue, J. 1999, *PASJ*, 51, 725.
doi:10.1093/pasj/51.5.725
- Wu, W.-B., Gu, W.-M., & Sun, M. 2022, *ApJ*, 930, 108.
doi:10.3847/1538-4357/ac6588
- Yang, X.-H., Yuan, F., Ohsuga, K., et al. 2014, *ApJ*, 780, 79. doi:10.1088/0004-637X/780/1/79
- Yang, H., Yuan, F., Kwan, T., et al. 2023, *MNRAS*, 523, 208. doi:10.1093/mnras/stad1444
- Yoshioka, S., Mineshige, S., Ohsuga, K., et al. 2022, *PASJ*, 74, 1378. doi:10.1093/pasj/psac076
- Zahra Zeraatgari, F., Mosallanezhad, A., Yuan, Y.-F., et al. 2020, *ApJ*, 888, 86. doi:10.3847/1538-4357/ab594f
- Zanni, C. & Ferreira, J. 2013, *A&A*, 550, A99.
doi:10.1051/0004-6361/201220168
- Zhu, Z., Stone, J. M., & Calvet, N. 2024, *MNRAS*, 528, 2883. doi:10.1093/mnras/stad3712